Journal of Power Sources 252 (2014) 235–243

Contents lists available at ScienceDirect

Journal of Power Sources

journal homepage: www.elsevier.com/locate/jpowsour

Hierarchical porous carbon derived from sulfonated pitch for electrical double layer capacitors

Yan Guo [a], Zhi-qiang Shi [b,**], Ming-ming Chen [a], Cheng-yang Wang [a,c,*]

[a] Key Laboratory for Green Chemical Technology of Ministry of Education, School of Chemical Engineering and Technology, Tianjin University, Tianjin 300072, PR China
[b] Laboratory of Fiber Modification and Functional Fiber, College of Materials Science and Engineering, Tianjin Polytechnic University, Tianjin 300387, PR China
[c] Synergetic Innovation Center of Chemical Science and Engineering (Tianjin), Tianjin 300072, PR China

HIGHLIGHTS

- Sulfonated pitch was utilized to synthesize hierarchical porous carbon.
- High BET specific surface area of 2602 m^2 g^{-1} was obtained with an activation agent to precursor ration of 1.5.
- The specific capacitance could be maintained at 157 F g^{-1} even at 100 A g^{-1}.
- Outstanding cyclic stability with a super high capacitance retention ratio of 98.4% after 10,000 cycles.

GRAPHICAL ABSTRACT

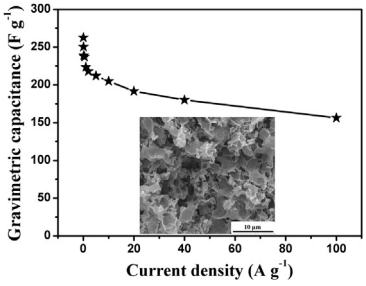

ARTICLE INFO

Article history:
Received 10 September 2013
Received in revised form
20 November 2013
Accepted 29 November 2013
Available online 11 December 2013

Keywords:
Electrical double layer capacitor
Hierarchical porous carbon
Sulfonated pitch
Functional groups

ABSTRACT

Hierarchical porous carbon (HPC) has been synthesized using sulfonated pitch as a precursor with a simple KOH activation process. Sulfonated pitch has a high content of oxygen-containing groups which enable it to be easily wetted in KOH solution and facilitate the activation process. The effect of the activation agent to precursor ratio on the porosity and the specific surface area is studied by nitrogen adsorption–desorption. A maximum specific surface area of 3548 m^2 g^{-1} is achieved with a KOH to sulfonated pitch ratio of 3 and this produces a structure with micro-, meso- and macropores. Among the various HPC samples, the sample prepared with an activation agent to precursor ratio of 1.5 exhibits the best electrochemical performance as an electrode in an electrical double layer capacitor (EDLC) in 6 M KOH electrolyte. Its gravimetric specific capacitance is 157 F g^{-1} at a current density of 100 A g^{-1} and it has a capacitance retention ratio of 98.4% even after 10,000 cycles. The sample also presents outstanding electrochemical performance in 1 M Li_2SO_4 and 1 M TEA BF_4/PC electrolytes. Thus, HPC derived from sulfonated pitch is a promising electrode material for EDLCs.

1. Introduction

Electrical double layer capacitors (EDLCs) have stimulated extensive interest due to their advantages of high power capability, superior reversibility and long cycle life, which are required for new energy storage devices [1,2]. Charge storage in EDLCs utilizes electrostatic adsorption of the electrolyte ions at the electrode–electrolyte interface [3]. An ideal electrode material is expected to

* Corresponding author. Key Laboratory for Green Chemical Technology of Ministry of Education, School of Chemical Engineering and Technology, Tianjin University, Tianjin 300072, PR China.
** Corresponding author.
E-mail addresses: guoyan0721@126.com (Y. Guo), shizhiqiang@tjpu.edu.cn (Z.-q. Shi), cywang@tju.edu.cn (C.-y. Wang).

0378-7753/$ – see front matter © 2013 Elsevier B.V. All rights reserved.
http://dx.doi.org/10.1016/j.jpowsour.2013.11.114

possess a large surface area, an optimal pore size distribution and excellent conductivity for fast transport of the electrolyte ions and charges [4].

Microporous activated carbons are the most common electrode material because of their high surface area, good conductivity, and chemical inertness [5]. Microporous activated carbon electrodes exhibit high specific capacitances at low current densities. However, the capacitance decreases dramatically with increasing current density. This is mainly caused by many small micropores and irregularly curved pores which slow down the ion transport rate and thus limit power storage. To solve this problem, activated carbons with controllable pore sizes and high surface areas are required.

Currently, hierarchical porous carbons (HPCs) with micro-, meso- and macropore structures have attracted much attention. In these materials the micropores provide abundant adsorption sites which are the primary contributors to the large specific capacitances [6]; the mesopores facilitate the diffusion of the electrolyte ions so they reach the available surface area and the macropores act as ion-buffering reservoirs to ensure adequate penetration of the electrolyte into the electrode materials [7]. In fact, the use of HPCs as electrode materials has been demonstrated to simultaneously achieve high energy and power densities.

The most common method to synthesize HPCs is the template method which has three steps: template replication, carbonization and removal of the template [8]. Various templates such as hierarchical porous silica monoliths [9] and powdery silica [10] have been used. For example, Kim et al. [11] used a beta zeolite as a hard template to synthesize HPC with micropores of 1 nm diameter and mesopores of 10–30 nm. Ma et al. [12] reported the synthesis of micro- and mesoporous carbons spheres by colloidal silica as template. Yamada et al. [13] used colloidal crystals as templates to synthesize 3D ordered porous carbons. Oschatz et al. [14] prepared the carbide-derived carbon materials (CDCs) containing micro-, meso-, and macropores through combining a soft-template approach with subsequent chlorine etching. This new synthesis route avoids the use of hard templates, thus the corresponding template removal process is avoided. Liang and Dai [15] reported the synthesis of highly ordered porous carbon by using self-assembled block copolymers as soft templates. In this method, the extra step of generating a template was unnecessary. Adelhelm et al. [16] used an organic polymer as the template to prepare a meso- and macroporous carbon using spinodal decomposition of the templates and a carbon precursor. Liu and co-workers [17] developed a new way to prepare nanoporous carbon using metal-organic frameworks as the template. The obtained nanoporous carbon with micro-, meso- and macropore structures exhibited remarkable electrochemical performance as an electrode of EDLC. However, all of the above methods contain complicated multistep procedures, which are tedious, cost and low yields, limiting their practical applications. Thus, new template-free methods are needed to synthesize HPCs. Lv et al. [18] reported the synthesis of hierarchical porous carbon foams from the bioresource banana peel through a self-template approach by utilizing its natural pore and zinc ions as the self-template.

In present work, sulfonated pitch (SP) is employed as the raw materials to prepare the HPCs. The SP contains a high concentration of oxygen-containing groups, providing many reactive sites for activation. More importantly, the presence of heteroatoms, e.g. S, O and N enhances the polarity of the carbon surface and increases the affinity of the surface for aqueous electrolytes. It is believed that sulfonated pitch is partly dissolved and partly dispersed in hydrosols [19]. This occurs through nano-scale contact between the reagents and the precursor, which should make it possible to prepare HPCs with large surface areas and well-developed porous structures. Moreover, the oxygen-containing groups in the sulfonated pitch are unstable and can decompose to CO_2 and CO during heat treatment, which can assist in creating additional pores [20]. These properties should enable sulfonated pitch a promising candidate for producing HPCs with the characteristics of preparation simplicity and easy scalability. Combing the advantage of commercially availability, sulfonated pitch precursor shows great potential in the energy storage field.

2. Experimental

2.1. Material preparation

Sulfonated pitch, purchased from Originchem Co., Ltd, was used as the raw material to prepare HPCs. Sulfonated pitch was added to KOH solutions with different KOH to precursor mass ratios and stirred for 1 h. The mixtures were dried at 80 °C for 12 h, and then transferred into a tube furnace and heat-treated at 800 °C for 2 h under a flow of nitrogen. After activation, the samples were washed three times with 1 M HCl solution. Then they were repeatedly rinsed by deionized water for three to five times until the pH of the washing solution was 7. Finally, the samples were dried at 120 °C for 12 h. The obtained samples were named HPC-*x* where *x* represents the weight ratio of solid KOH to sulfonated pitch.

2.2. Characterization

The surface of the samples was characterized by X-ray photoelectron spectroscopy (XPS) using a PHI-1600ESCA electron system (America PE Company) with Al Kα (1486.6 eV) radiation. Fourier transform infrared spectrometry (FT-IR) was carried out with a Nicolet Magna-IR 560 FTIR spectrometer over the wavenumber range of 4000–400 cm^{-1}. Thermogravimetric analysis (TGA) was performed using a TA-50 instrument in a nitrogen atmosphere. Raman spectra were measured by a Renishaw MKI-2000 Raman microscope using an Ar ion laser (488 nm) as the excitation source. The specific surface areas and the pore structures of the samples were examined by nitrogen adsorption measurements at 77 K (ASAP 2020, Micromeritics, USA). Before the measurements, the samples were degassed at 300 °C for 5 h under vacuum. The specific surface area and the total pore volume were calculated using the Brunauer–Emmett–Teller (BET) theory over a relative pressure (P/P_0) range from 0.1 to 0.3 and the volume of nitrogen adsorbed at a relative pressure of 0.99, respectively. The micropore volume was calculated using the t-plot method, and the surface areas and pore volumes of the mesoporous were analyzed according to the Barrett–Joyner–Halenda (BJH) method. The pore size distributions were studied using the nonlocal density function theory (NLDFT) model assuming slit-shaped pores. The microstructures of the HPCs were investigated using field emission scanning electron microscopy (FESEM, Nano430) and high-resolution transmission electron microscopy (HRTEM, Philips Tecnai G2 F20). The samples were deposited on the conductive paste, subsequently coated with gold using a gold sputtering device for field emission scanning electron microscopy and dispersed in absolute ethanol with ultrasonication for 30 min, then dropped onto copper mesh for high-resolution transmission electron microscopy.

2.3. EDLC construction and electrochemical measurements

The obtained HPC material (80 wt%), acetylene black (10 wt%) and poly(tetrafluoroethylene) (10 wt%) were homogenized in a mortar, rolled into an electrode membrane (13 mm in diameter, 100 μm thick). The characterization of the electrode material was performed using a symmetric EDLC cell composed of two HPC-

based composite electrodes with equal mass of active materials and a three-electrode cell with platinum foil and saturated calomel electrode as counter electrode and reference electrode, respectively. The electrochemical behaviors of the electrode working in three types of electrolytes were investigated. The electrolytes were 6 M KOH aqueous solution, 1 M Li_2SO_4 aqueous solution and 1 M tetraethylammonium tetrafluoroborate salt solution in propylene carbonate (TEA BF_4/PC), respectively. The EDLC cell was placed into a vacuum oven at room temperature for 24 h before the electrochemical measurements to make sure there was good contact between the electrode and the electrolyte.

The electrochemical performances of the HPC electrode materials were measured using galvanostatic charge/discharge cycles, cyclic voltammetry (CV) and electrochemical impedance spectroscopy (EIS). The galvanostatic charge–discharge tests were conducted at different current densities using a Land Battery Tester (Wuhan, China). The gravimetric capacitance C_g of a single electrode is calculated according to the discharge part of galvanostatic charge/discharge curves using the equation $C_g = 2I\Delta t/(m\Delta V)$, where I is the discharge current, Δt is the discharge time, ΔV is the voltage drop upon discharge excluding the IR drop, and m is the mass of active material in the electrode. At the beginning of the discharge, there is a sudden drop of potential associated with the ohmic resistance (R) of the cell which can be calculated according to the equation [21] $R = (V_{charge} - V_{discharge})/2I$, where V_{charge}, $V_{discharge}$ and I represent the voltage at the end of the charge, the voltage at the beginning of the discharge, and the discharge current, respectively.

CV and EIS were performed on an electrochemical workstation (PARSTAT 2273, Princeton Applied Research, USA). The CV analyses were investigated with sweep rates from 2 to 200 mV s^{-1}. The CV tests were also used to determine the specific capacitance. The calculation was performed using the equation $C = (\int I dV)/(\upsilon XV)$, where C represents for the gravimetric specific capacitance (F g^{-1}) or volumetric specific capacitance (F cm^{-3}), I is the current, V is the potential difference, X is the mass (g) of the active material in one electrode or volume (cm^3) of the electrode, and υ is the scan rate (mV s^{-1}). The impedance measurements were carried out at an open circuit voltage over a wide frequency range (100 kHz–10 mHz). The capacitor using 6 M KOH, 1 M Li_2SO_4 and 1 M TEA BF_4/PC as electrolytes was operated within a potential range of 0–1, 0–1.6 and 0–2.7 V, respectively. The energy density and average power density of the capacitor is calculated using the equations: $E = C_g\Delta V^2/2$ and $P = E/\Delta t$, where C_g refers to gravimetric capacitance of the capacitor calculated from galvanostatic charge/discharge tests at different current densities.

3. Results and discussion

3.1. Material characterization

Information about the chemical state of the elements anchored in the sulfonated pitch surface was obtained from XPS. Wide scan spectra of the sulfonated pitch and the HPC samples are shown in Fig. 1a. The oxygen O 1s peak located at 532 eV is remarkably strong in the sulfonated pitch spectrum, indicating a high concentration of oxygen-containing groups. The sulfur S 2p spectra of the samples are displayed in Fig. 1b. There are two distinctive peaks in the sulfonated pitch spectrum. The strong peak at 168–169 eV represents sulfur in a higher oxidation state (sulfonates, sulfites, sulfates, etc) whereas the weak peak at 164 eV corresponds to sulfur attached to a carbon or an oxygen atom [22]. In the HPC spectra, these peaks disappeared, which clearly demonstrates that most of the S atoms were removed by the activation.

In the C 1s spectrum of the sulfonated pitch (Fig. 1c), there are peaks for the different types of functional groups, namely C–C, C=C, and C–H bonds (284.6 eV), C–O bonds (285.7 eV), and O–

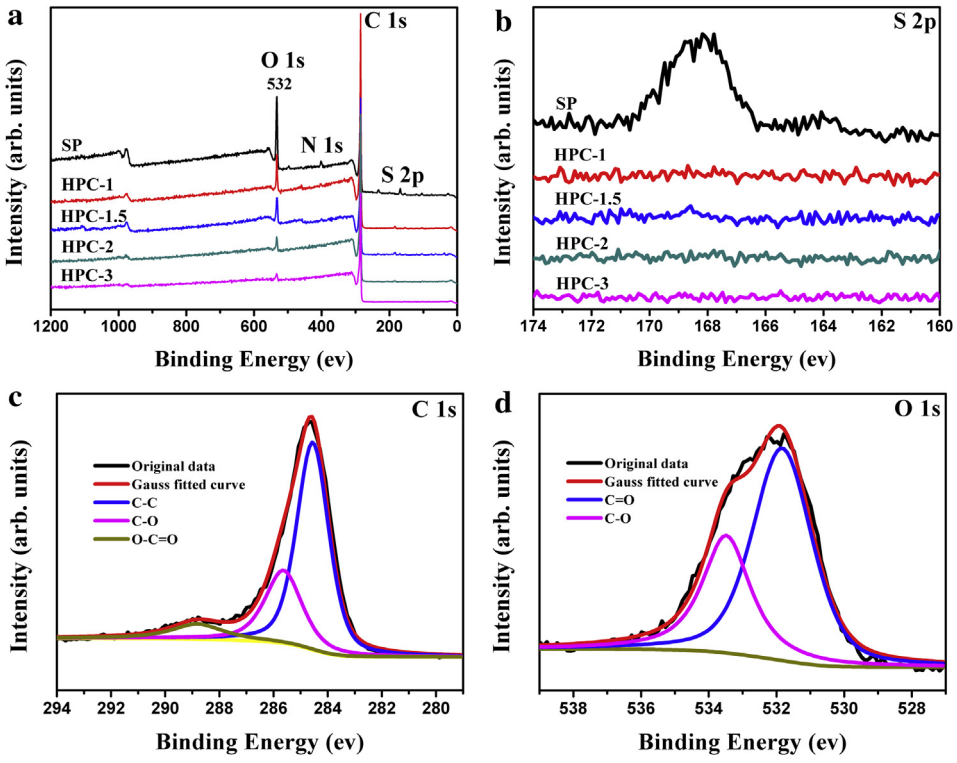

Fig. 1. (a) XPS wide scan spectra and (b) XPS S 2p spectra of the sulfonated pitch and HPC samples; (c) C 1s and (d) O 1s XPS spectra of the sulfonated pitch.

C=O bonds (288.9 eV), with area fractions of 0.64, 0.27, and 0.09, respectively [23]. The O 1s spectrum of the sulfonated pitch (Fig. 1d) can be fitted into two major component peaks. The peak at 531.8 eV is attributed to C=O bonds and the 533.5 eV peak is due to C–O. These observations demonstrate that the sulfonated pitch consists of aromatic carbon sheets with $-SO_3H$, –COOH and –OH functional groups.

FT-IR spectra were also recorded to evaluate the functional groups in the sulfonated pitch and HPC samples and are shown in Fig. 2. The peak around 3440 cm^{-1} corresponds to the O–H stretching mode of the hydroxyl functional groups; the band at about 1720 cm^{-1} can be assigned to ketone or carboxylic acid C=O stretching vibrations and the band at 1600 cm^{-1} is aromatic C=C stretching vibrations [24]. The peaks at 1440 and 1380 cm^{-1} are for aliphatic C–H bending vibrations [25]. The absorption peaks at 1175 and 1040 cm^{-1} can be ascribed to the asymmetric and symmetric vibrations of the SO_3 group, respectively, and the peak at 620 cm^{-1} may be related to the stretching vibration of the C–S bonds [19]. The sharp peak at 1120 cm^{-1} probably corresponds to the C–O stretching mode [26]. For the HPCs, the spectra are essentially the same, indicating that the structures are the same. The intensities of the sulfonic acid group and carboxyl group peaks are much weaker in the HPC spectra than in the sulfonated pitch spectrum. In addition, the peak intensity of the C–O group decreased dramatically in the HPC spectra. These findings show that most of the functional groups were removed during the KOH activation process, which is consistent with the XPS results.

The thermal stability of the sulfonated pitch from room temperature to 1000 °C was studied by TGA under flowing N_2 and the results are shown in Fig. 3. From room temperature to 100 °C there is a slight weight loss which is due to the removal of the adsorbed water molecules. The mass loss between 300 and 500 °C is significant and this is a typical temperature range for the thermal decomposition of the $PhSO_3H$ groups in the sulfonated pitch [27]. The thermal decomposition of the $PhSO_3H$ contains of two steps: first, a dehydration reaction occurs which forms the sulfonyl bridges between the adjacent aromatic rings and then the sulfonyl bridges are pyrolyzed, forming polyaromatic structures [28]. The mass loss between 700 and 1000 °C is small (3 wt%), which can be attributed to the increase of the polyaromatic structures. The total weight loss is about 39.7 wt% at 1000 °C.

Fig. 4 shows Raman spectra of the HPC samples. Two broad peaks around 1580 cm^{-1} (G-band) from graphitic carbon and 1347 cm^{-1} (D-band) from disordered carbon were observed. The integrated intensities ratio of the D band to the G band (I_D/I_G) is a useful parameter for the characterization of the graphitization degree. As shown in Fig. 4b, the high ratios (I_D/I_G) reveal the amorphous character and a high degree of disorder or defects of the obtained HPCs [29]. The ratio (I_D/I_G) increased with the activation agent to precursor ratio, exhibiting a noticeable decrease in structural order and thus electrical conductivity.

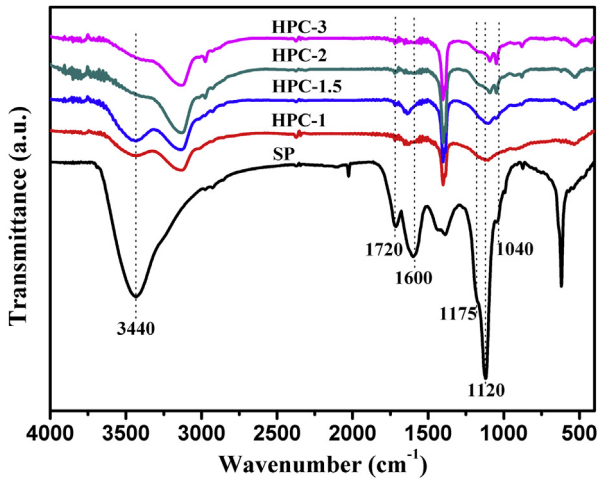

Fig. 2. FTIR spectra of the sulfonated pitch and HPC samples.

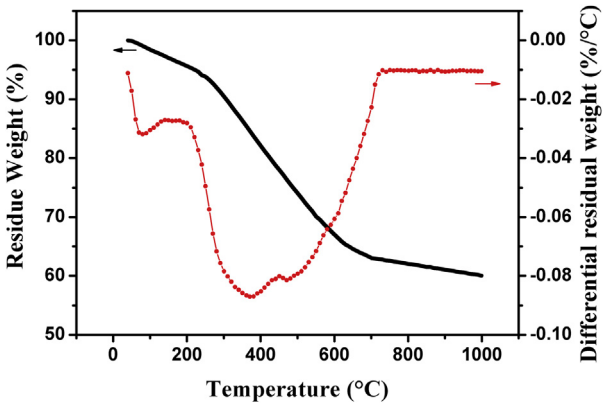

Fig. 3. Weight loss of the sulfonated pitch under a N_2 atmosphere.

3.2. Characterization of the porous structures of the HPCs

The N_2 adsorption isotherms and pore size distribution curves of the HPCs are presented in Fig. 5. All isotherms are type IV curves (based on IUPAC classification) with a typical hysteresis loop in the intermediate relative pressure range. The adsorption capacity of the HPCs increased with the activation agent to precursor ratio. The BET surface area and pore structure parameters are shown in Table 1. The total pore volume and specific surface area also increased with the activation agent to precursor ratio. HPC-3 had the highest specific area (3548 $m^2\ g^{-1}$) and porosity volume (2.45 $cm^3\ g^{-1}$). When the activation agent to precursor ratio was only 1.5, the specific surface area could reach 2602 $m^2\ g^{-1}$.

The high surface areas are the result of the chemical nature of the sulfonated pitch. Because of its hydrophilic nature, the sulfonated pitch can be readily dissolved and dispersed in KOH solution, which favors homogeneous activation [19]. Further, the heteroatoms in the sulfonated pitch are chemically instable which provide more “active sites” for activation [30]. Thus, the surface functional groups of the sulfonated pitch can improve the efficiency of the activating agent and have a meaningful contribution to the high BET surface area.

In EDLCs, the surface area of the material is an important parameter. However specific capacitance is also governed by how easily the electrolyte can access the pores of the materials. Micropores can create bottlenecks which prevent solvated ions from entering into interior surfaces of the pores. According to E. Raymundo-Piñero et al. [31] the optimal pore size for an effective double layer formation in an aqueous electrolyte is around 0.7 nm.

It can be seen from Fig. 5b that all of HPCs exhibit obvious hierarchical porous structures. The presence of ultrafine micropores (<1 nm) with pore width peaks at 0.6 and 0.8 nm and micropores (1–2 nm) with a maximum peak at 1.2 nm should provide a highly ion-accessible surface which is crucial for the formation of an electrical double layer capacitor [6]. The mesopores (2–50 nm) are primarily in the range of 2–5 nm, which should provide a channel for fast ion transport and a low resistance for charge transfer. Furthermore, there is a very broad pore width peak ranging from 10 to 50 nm. The macropores (>50 nm) with a pore width peak at 125 nm should play an important role as ion-buffering reservoirs [7].

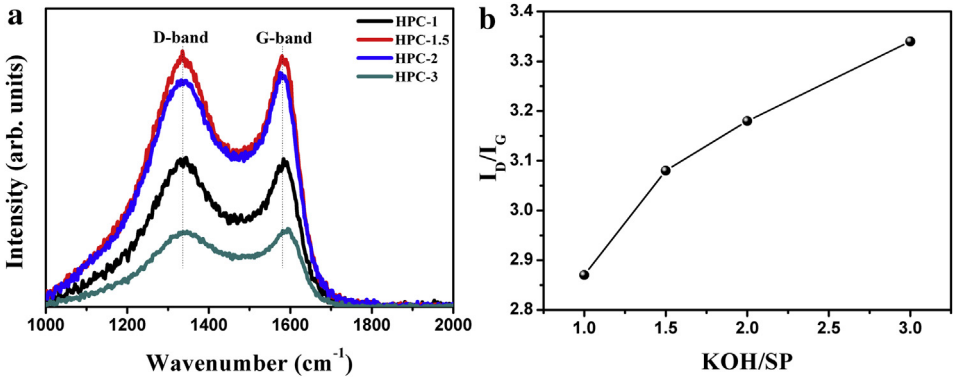

Fig. 4. (a) Raman spectra and (b) I_D/I_G ratio of HPC samples as a function of activation agent to precursor ratio.

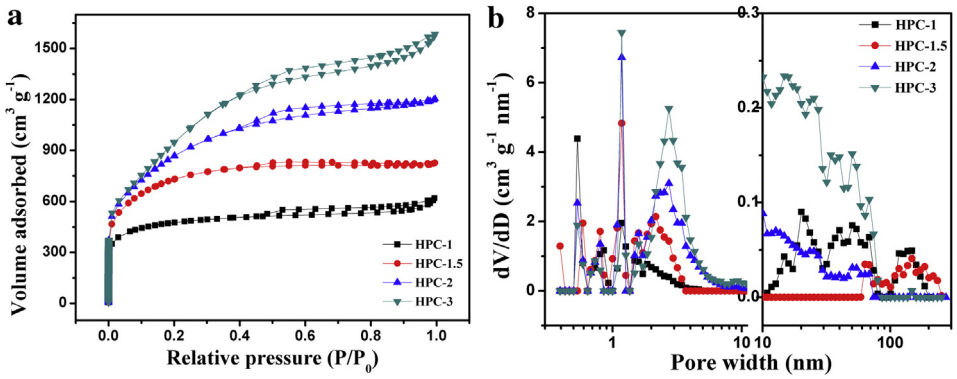

Fig. 5. (a) N_2 adsorption/desorption isotherms and (b) pore size distribution for the HPC samples.

For HPC-1 the maximum pore width peak is at 0.6 nm. As the activation agent to precursor ratio increased, the pore volumes of the micropores decreased whereas the mesopores volumes increased and the mesopores peak maximum moved from 2 to 3 nm. This may be due to the micropores growing larger or collapsing, which led to the formation of small mesopores and the generation of more pores.

The porous structure was further verified by FESEM and HRTEM. The FESEM image of HPC-1.5 in Fig. 6a shows the microstructure of the porous carbon with numerous interconnected macropores with pore sizes of 1–5 μm. The HRTEM image in Fig. 6b shows that HPC-1.5 is amorphous and has a highly disordered pore structure. Furthermore, there are abundant micropores along with the mesoporous channel walls, indicating the formation of a continuous three-dimensional pore network. This is consistent with the DFT pore size distribution results.

3.3. Electrochemical characterization

Fig. 7 shows the electrochemical performances of HPCs working with 6 M KOH solution. Charge–discharge tests were used to study the effect of the activation agent to precursor ratio on the specific capacitances of the HPC samples. The charge–discharge curves for the HPC electrodes at a current density of 10 A g^{-1} are shown in Fig. 7a. All curves are nearly triangular in shape which is typical behavior for capacitive electrodes. The HPC-1 sample has a larger ohmic-drop and a smaller specific capacitance than the other samples. This can be ascribed to the ultrafine micropores in that sample, which are not favorable for fast diffusion of the electrolyte ions. Micropores limit the motion of the ions, and thus lead to the inner parts of the electrode being inaccessible at high charge/discharge rates. This behavior did not occur in the other samples because of their higher mesopore content. The ohmic resistance (R) of the HPC-1.5 electrode is 0.59 Ω, which is the smallest among all the HPC electrodes. This result indicates that the HPC-1.5 electrode has the best ionic conductivity and electrical conductivity properties.

When the activation agent to precursor ratio was increased from 1 to 1.5, the gravimetric specific capacitance increased rapidly from 157 to 205 F g^{-1}. When the ratio was further increased to 2 or 3, there was no further increase in the capacitance. The increase in capacitance is mainly due to the relatively high specific area and the reasonably porous structure in HPC-1.5 which provides enough surface sites for electrochemical double layer formation.

Furthermore, the volumetric specific capacitance is much more important for practical application. As shown in Table 1, the density of the HPCs decrease with increasing activation agent to precursor ratio, varying in the range of 0.22–0.47 g cm^{-3}. Compared with other porous materials reported in the literature [32,33], the density of the HPCs is a little lower, which can be ascribed to the large pore volume. The volumetric specific capacitances of samples at different scan rates are shown in Fig. 7b. HPC-1, with the lowest V_{tot}

Table 1
Properties of the hierarchical porous carbons.

Samples	S_{BET} (m^2 g^{-1})	S_{meso} (m^2 g^{-1})	V_{total} (cm^3 g^{-1})	V_{micro} (cm^3 g^{-1})	V_{meso} (cm^3 g^{-1})	Density (g cm^{-3})
HPC-1	1644	317	0.96	0.43	0.38	0.47
HPC-1.55	2602	556	1.28	0.34	0.44	0.41
HPC-2	3177	1339	1.86	0.29	1.20	0.33
HPC-3	3548	2103	2.45	0.20	2.05	0.22

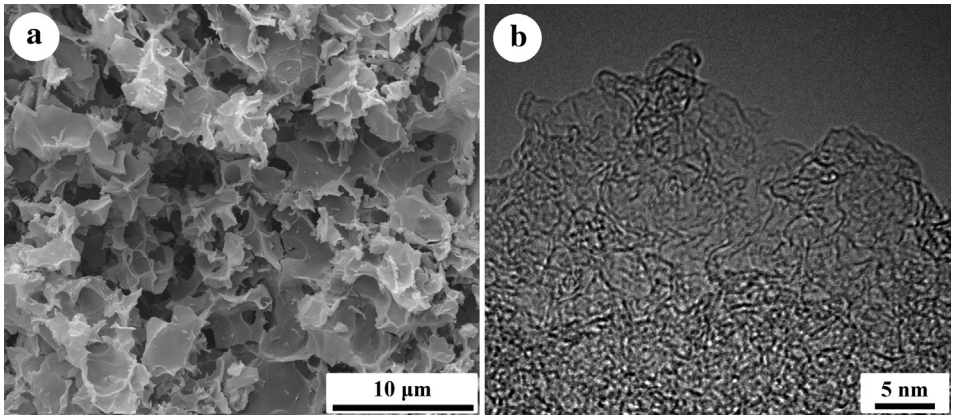

Fig. 6. (a) FESEM images and (b) HRTEM images of the HPC-1.5 sample.

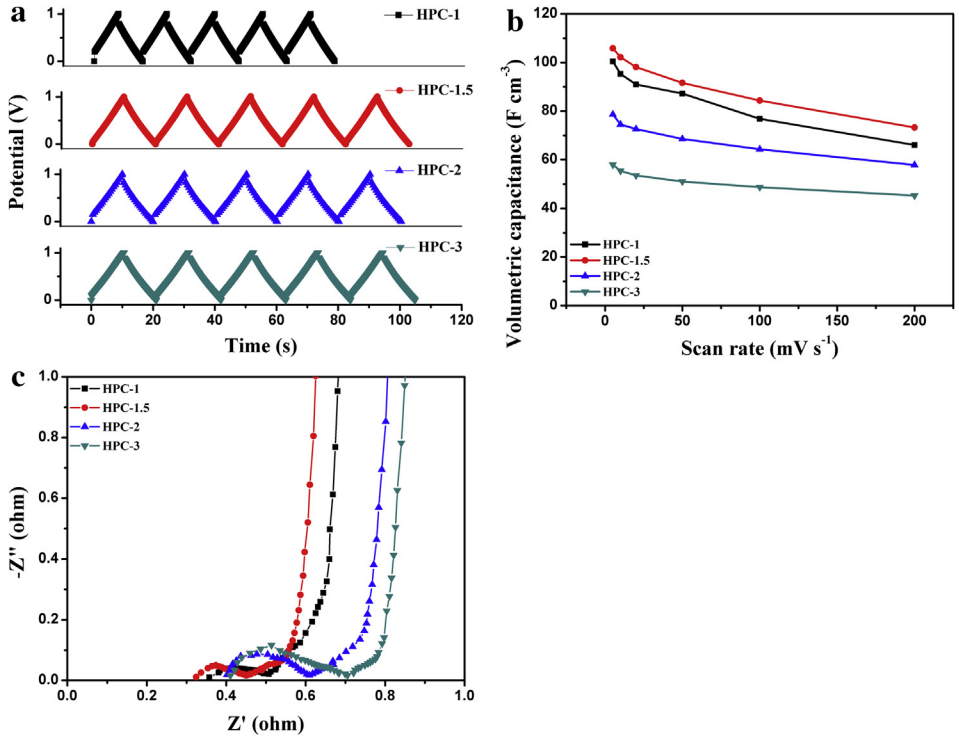

Fig. 7. (a) Galvanostatic charge–discharge curves at a current density of 10 A g^{-1}, (b) the volumetric capacitance of the single electrode as a function of the scan rate and (c) Nyquist plots in the frequency range of 10 mHz–100 kHz for the HPC electrodes in a solution containing 6 M KOH.

(0.96 cm^3 g^{-1}) among all the HPC samples, shows a high volumetric capacitance of 100 F cm^{-3} at a scan rate of 5 mV s^{-1}. On the contrary, for the HPC-3 electrode, the large pore volume (2.45 cm^3 g^{-1}) results in the low electrode density (0.22 g cm^{-3}) and thus relatively low volumetric capacitance. HPC-1.5 balances porosity and density, showing the optimized volumetric performance.

The Nyquist plots in Fig. 7c show that all the electrodes have similar impedance behaviors. All the plots have a single small semicircle, a line with a slope close to 45°, and an almost vertical line at the high, middle, and low frequency ranges, respectively. This behavior is indicative of excellent EDLC performance. In the low frequency range, the straight line is nearly parallel to the imaginary axis (Z″), which suggests good supercapacitor capacitive behavior. The portion of the curve with the 45° slope is called the Warburg resistance and corresponds to the diffusive resistance of the ions in the electrode. Except for HPC-1, the Warburg regions for all the electrodes are small which means the porous structure provides a channel that is favorable for the access of the electrolyte ions and for fast ion transport.

In the high frequency region, the intersection of the semicircle with the real axis depends on the internal resistance which includes the intrinsic resistance of the active material, the resistance of the electrolyte solution and the contact resistance of the active material/current collector [34]. The HPC-1.5 electrode curve crosses the real axis at 0.3 Ω, which is the smallest value among the tested electrodes. At the same time the smaller semicircle diameter for the HPC-1.5 curve means a smaller charge transfer resistance, suggesting that HPC-1.5 has high electrical conductivity and good power characteristics [35]. This result is in good agreement with the charge–discharge curves of the HPC electrodes in Fig. 7a.

The semicircle diameter of the HPC-3 electrode is larger than the other electrodes. This lower conductivity may be due to excessive KOH

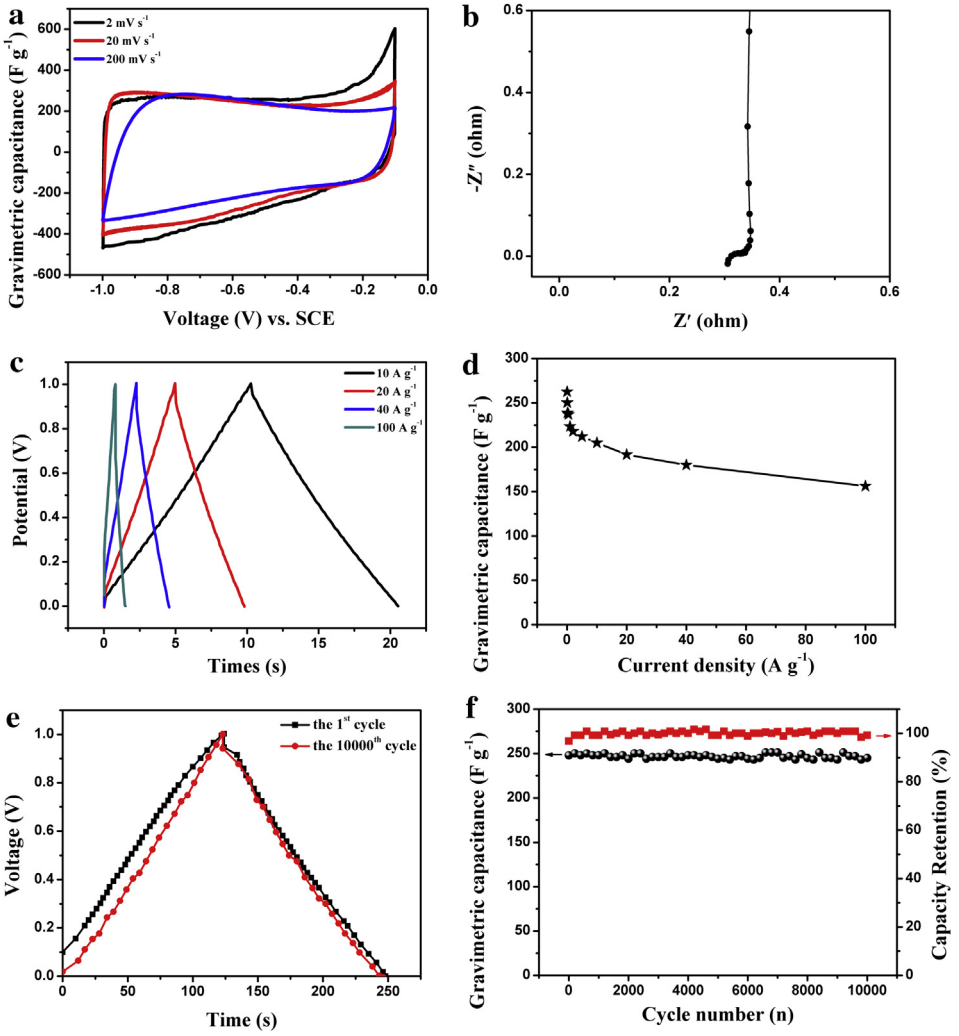

Fig. 8. Electrochemical characterization of the HPC-1.5 electrode in a 6 M KOH solution: (a) CV curves recorded at different scan rates and (b) Nyquist plots in the frequency range of 10 mHz–100 kHz in a three-electrode cell; (c) galvanostatic charge–discharge curves at different current densities, (d) effect of the current density on gravimetric specific capacitance, (e) galvanostatic charge–discharge curves at the 1st and the 10,000th cycle, (f) cycle performance at a current density of 1 A g^{-1} in a symmetrical two-electrode cell.

activation which leads to some degree of discontinuity in the porous structure [36]. The porous structure not only determines the ion diffusion process but also affects the electrical conductivity of the carbon materials. Larger surface areas and pore sizes result in lower conductivities [3]. Compared with HPC-1.5 (S_{BET} = 2602 m^2 g^{-1}), HPC-3 (3548 m^2 g^{-1}) has a higher surface area which is favorable for a larger gravimetric specific capacitance, but detrimental to the electrical conductivity, and the subsequent rate performance.

These results show that among the tested electrodes, HPC-1.5 is the most promising electrode material for EDLC applications. This is due to its low internal resistance, its excellent conductivity, its fast ion diffusion, and the low consumption of activating agents. Therefore, HPC-1.5 was selected for the subsequent electrochemical measurements.

The electrochemical behavior of the HPC-1.5 electrode was investigated in two- and three-electrode cells with a solution containing 6 M KOH. In Fig. 8a, CV curves were obtained from the three-electrode cell. At a slow scan rate (2 mV s^{-1}), there is a noticeable peak at −0.1 V (vs. SCE), which is related to the redox reactions. With the increase of scan rate, the gravimetric specific capacitance decreased from 277 F g^{-1} at 2 mV s^{-1} to 197 F g^{-1} at 200 mV s^{-1}. The well preserved specific capacitance indicates unrestricted diffusion of ions in the HPC-1.5 sample. The Nyquist plot (Fig. 8b) performed in a three-electrode cell reveals similar tendencies as observed in a two-electrode cell.

Fig. 8c displays the charge–discharge curves of HPC-1.5 at current densities of 10–100 A g^{-1} in a two-electrode cell. The linear symmetric profiles indicate that the HPC-1.5 electrode has a high Coulombic efficiency and excellent reversibility. The gravimetric specific capacitance values of HPC-1.5 at different current densities are shown in Fig. 8d. As the current density increased, the capacitance decreased slightly. The capacitance was 263 F g^{-1} at a current density of 0.05 A g^{-1} and dropped to 212 F g^{-1} when current density was increased to 5 A g^{-1}; when the current density was further increased, the capacitance decreased slowly. Fortunately, even when the current density was as high as 100 A g^{-1}, the sample still exhibited a high gravimetric specific capacitance of 157 F g^{-1}. A stable specific capacitance at a high current density indicates excellent rate performances which can be ascribed to an optimum pore size and a moderate specific surface area. These factors provide short diffusion routes and low-resistance for the ions to pass through the porous particles [37].

The durability of the EDLC was studied by repeating the charge/discharge test at a current density of 1 A g^{-1} for 10,000 cycles. Compared with the first cycle, there were little changes at the 10,000th cycle (Fig. 8e). As seen in Fig. 8f, there was negligible

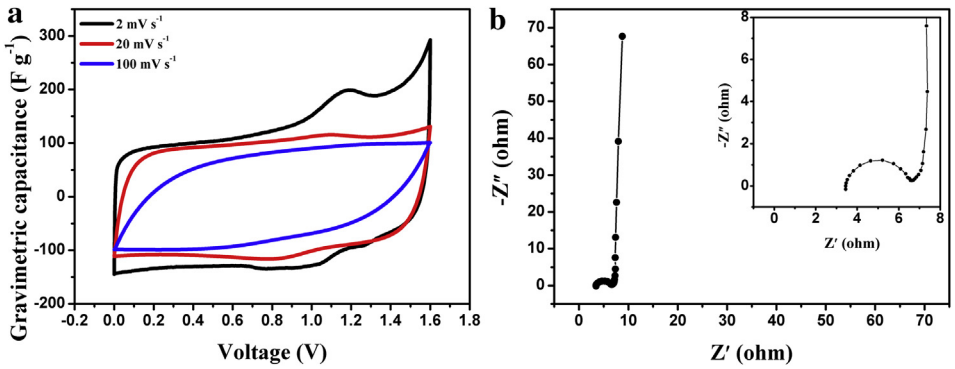

Fig. 9. Electrochemical properties of the HPC-1.5 electrode in a 1 M Li_2SO_4 solution operating within a potential range of 0.0 and 1.6 V: (a) CV curves at different scan rates, (b) Nyquist plots in the frequency range of 10 mHz–100 kHz.

capacitance degradation. The gravimetric specific capacitance decreased slightly and stabilized at 245 F g^{-1} after 10,000 cycles with a super high capacitance retention ratio of 98.4%. This demonstrates excellent electrochemical stability.

Apart from high power density, energy density must be considered, which is greatly affected by the operational voltage range. Therefore, it is necessary to investigate the application of the HPC-1.5 electrode in a wider voltage range in aqueous media. A symmetric capacitor working in 1 M Li_2SO_4 solution was fabricated. The visible hump at 1.2 V revealed by CV measurements (Fig. 9a) may result from the electro-oxidation of hydrogen adsorbed in HPC [38]. When the voltage is beyond 1.4 V, another peak can be observed, which is related with electrochemical oxidation of the positive electrode [39]. At a scan rate of 200 mV s^{-1}, redox peaks are disappeared because the side reactions are invisible [40]. The Nyquist plot (Fig. 9b) also confirms the capacitive behavior. The gravimetric specific capacitance is 204 F g^{-1} at 2 mV s^{-1}, slightly lower than that in KOH solution.

In addition, the electrochemical performance of the HPC-1.5 electrode was also investigated in 1 M TEA BF_4/PC solution. The CV curves at different scan rates are given in Fig. 10a. The curve was approximately rectangular without any redox peaks at scan rate of 2 mV s^{-1}, which is characteristic of a pure capacitive behavior. The gravimetric capacitance could reach 159 F g^{-1} at a scan rate of 2 mV s^{-1}. The Nyquist plot (Fig. 10b) contained a semicircle at high frequency and a nearly vertical line at low frequency. The charge–discharge curves (Fig. 10c) were triangular with a small decrease in IR at a current density of 1 A g^{-1}, showing a good capacitive behavior. Fig. 10d shows the Ragone plot of the symmetric capacitor. When using KOH as electrolyte, the energy and the power density were 5.4 Wh kg^{-1} and 27.8 kW kg^{-1} at a current density of 100 A g^{-1}, respectively, exhibiting an outstanding power

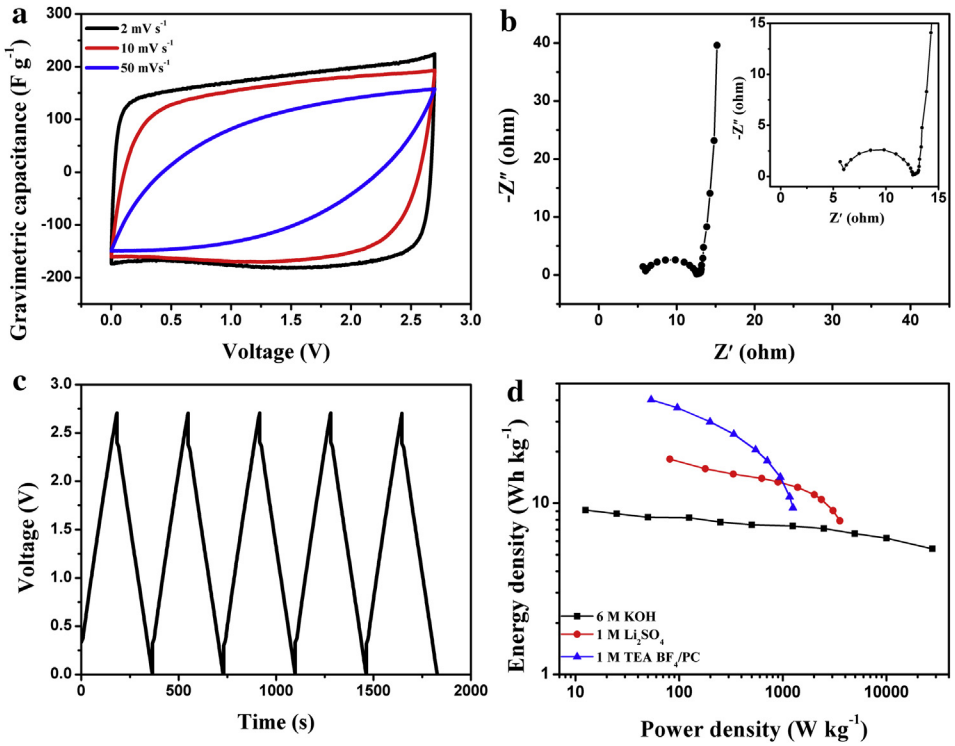

Fig. 10. Electrochemical properties of the HPC-1.5 electrode in a 1 M TEA BF_4/PC solution operating within a potential range of 0.0 and 2.7 V: (a) CV curves at different scan rates, (b) Nyquist plots in the frequency range of 10 mHz–100 kHz, (c) galvanostatic charge–discharge curves at a current density of 1 A g^{-1}. (d) Ragone plot of symmetric capacitors based on different electrolytes.

performance. However, the key disadvantage is that the limited operating voltage range (1.0 V) leads to low energy density. In contrast, the energy density is around 20 Wh kg^{-1} at a current density of 1 A g^{-1} based on organic electrolyte. Despite the smaller capacitance values in Li_2SO_4 solution compared to using KOH as electrolyte, the former demonstrates a higher energy density combined with a satisfactory rate performance.

4. Conclusions

In conclusion, high conductivity HPCs with a large surface area and with micro-, meso- and macroporous structures have been prepared by the simple KOH activation of sulfonated pitch. The S_{BET} and V_{tot} of the HPCs increased with the activation agent to precursor ratio. The optimum activation agent to precursor ratio was determined to be 1.5, which resulted in a specific surface area of 2602 m^2 g^{-1} and a porosity volume of 1.28 cm^3 g^{-1}. A symmetrical EDLC using the HPC-1.5 sample as the electrode showed superior capacitive behavior. When using 6 M KOH as electrolyte, the charge–discharge curve maintained a triangular sharp at a current density of 100 A g^{-1} and the electrode exhibited a low ohmic resistance with excellent rate capability. The gravimetric capacitance was 263 F g^{-1} at a current density of 0.05 A g^{-1}, and could be maintained at 157 F g^{-1} even at 100 A g^{-1}. There was no observable decrease in the capacitance after 10,000 charge–discharge cycles. A symmetric supercapacitor worked with 1 M TEA BF_4/PC electrolyte exhibited a high energy density of up to 20 Wh kg^{-1} at a current density of 1 A g^{-1}. When using 1 M Li_2SO_4 as electrolyte, the symmetric supercapacitor exhibited an improved cell voltage window and thus higher energy density than in 6 M KOH solution.

HPCs derived from sulfonated pitch not only can achieve high capacity but also can provide a continuous three-dimensional pore network for fast ionic motion, resulting in high energy density and power output. Thus, HPCs derived from sulfonated pitch exhibit great potential for applications in energy storage. Additionally, a convenient and economic preparation method makes the HPCs prepared from sulfonated pitch an extremely attractive electrode material for EDLCs.

Acknowledgments

This research was supported by the National High Technology Research and Development Program of China (863) (2011AA11A232, 2013AA050905), the National Nature Science Foundation of China (51172160, 50902102) and NSF of Tianjin City (11JCYBJC07500).

References

[1] P. Simon, Y. Gogotsi, Nat. Mater. 7 (2008) 845.
[2] M. Inagaki, H. Konno, O. Tanaike, J. Power Sources 195 (2010) 7880.
[3] E. Frackowiak, F. Béguin, Carbon 39 (2001) 937.
[4] Y.P. Zhai, Y.Q. Dou, D.Y. Zhao, P.F. Fulvio, R.T. Mayes, S. Dai, Adv. Mater. 23 (2011) 4828.
[5] A. Stein, Z.Y. Wang, M.A. Fierke, Adv. Mater. 21 (2009) 265.
[6] J. Chmiola, G. Yushin, Y. Gogotsi, C. Portet, P. Simon, P.L. Taberna, Science 313 (2006) 1760.
[7] D.W. Wang, F. Li, M. Liu, G.Q. Lu, H.M. Cheng, Angew. Chem. 120 (2008) 379.
[8] J.E. Hampsey, Q.Y. Hu, L. Rice, J.B. Pang, Z.W. Wu, Y.F. Lu, Chem. Commun. (2005) 3606.
[9] A.H. Lu, J.H. Smått, S. Backlund, M. Lindén, Microporous Mesoporous Mater. 72 (2004) 59.
[10] A. Taguchi, J.H. Smått, M. Lindén, Adv. Mater. 15 (2003) 1209.
[11] K. Kim, M. Choi, R. Ryoo, Carbon 60 (2013) 175.
[12] X.M. Ma, M.X. Liu, L.H. Gan, Y.H. Zhao, L.W. Chen, J. Solid State Electrochem. 17 (2013) 2293.
[13] H. Yamada, H. Nakamura, F. Nakahara, I. Moriguchi, T. Kudo, J. Phys. Chem. C 111 (2007) 227.
[14] M. Oschatz, L. Borchardt, M. Thommes, K.A. Cychosz, I. Senkovska, N. Klein, R. Frind, M. Leistner, V. Presser, Y. Gogotsi, S. Kaskel, Angew. Chem. Int. Ed. 51 (2012) 7577.
[15] C.D. Liang, S. Dai, J. Am. Chem. Soc. 128 (2006) 5316.
[16] P. Adelhelm, Y.S. Hu, L. Chuenchom, M. Antonietti, B.M. Smarsly, J. Maier, Adv. Mater. 19 (2007) 4012.
[17] B. Liu, H. Shioyama, T. Akita, Q. Xu, J. Am. Chem. Soc. 130 (2008) 5390.
[18] Y.K. Lv, L.H. Gan, M.X. Liu, W. Xiong, Z.J. Xu, D.Z. Zhu, D.S. Wright, J. Power Sources 209 (2012) 152.
[19] H. Preiss, G. Oliew, K. Szulzewsky, Fuel 73 (1994) 243.
[20] B.K. Pradhan, N.K. Sandle, Carbon 37 (1999) 1323.
[21] R.M. Lago, S.C. Tsang, K.L. Lu, Y.K. Chen, M.L.H. Green, J. Chem. Soc. Chem. Commun. (1995) 1355.
[22] J.W. Gu, X.L. Yang, H.S. Zhu, Mater. Sci. Eng. C 20 (2002) 199.
[23] G.X. Zhao, L. Jiang, Y.D. He, J.X. Li, H.L. Dong, X.K. Wang, W.P. Hu, Adv. Mater. 23 (2011) 3959.
[24] M. Acik, C. Mattevi, C. Gong, G. Lee, K. Cho, M. Chhowalla, Y.J. Chabal, ACS Nano 4 (2010) 5861.
[25] H.M. Zhu, J.H. Yan, X.G. Jiang, Y.E. Lai, K.F. Cen, J. Hazard. Mater. 153 (2008) 670.
[26] U.J. Kim, C.A. Furtado, X.M. Liu, G.G. Chen, P.C. Eklund, J. Am. Chem. Soc. 127 (2005) 15437.
[27] X.Y. Liu, M. Huang, H.L. Ma, Z.Q. Zhang, J.M. Gao, Y.L. Zhu, X.J. Han, X.Y. Guo, Molecules 15 (2010) 7188.
[28] G. Hasegawa, K. Kanamori, K. Nakanishi, T. Hanada, Carbon 48 (2010) 1757.
[29] M. Rose, Y. Korenblit, E. Kockrick, L. Borchardt, M. Oschatz, S. Kaskel, G. Yushin, Small 7 (2011) 1108.
[30] J. Wang, M.M. Chen, C.Y. Wang, J.Z. Wang, J.M. Zheng, J. Power Sources 196 (2011) 550.
[31] E. Raymundo-Piñero, K. Kierzek, J. Machnikowski, F. Béguin, Carbon 44 (2006) 2498.
[32] Y. Korenblit, M. Rose, E. Kockrick, L. Borchardt, A. Kvit, S. Kaskel, G. Yushin, ACS Nano 4 (2010) 1337.
[33] B. Xu, F. Wu, S. Chen, Z.M. Zhou, G.P. Cao, Y.S. Yang, Electrochim. Acta 54 (2009) 2185.
[34] L.F. Lai, H.P. Yang, L. Wang, B.K. Teh, J.Q. Zhong, H. Chou, L.W. Chen, W. Chen, Z.X. Shen, R.S. Ruoff, J.Y. Lin, ACS Nano 6 (2012) 5941.
[35] L. Yang, S. Cheng, Y. Ding, X.B. Zhu, Z.L. Wang, M.L. Liu, Nano Lett. 12 (2012) 321.
[36] L.L. Zhang, X. Zhao, M.D. Stoller, Y.W. Zhu, H.X. Ji, S. Murali, Y.P. Wu, S. Perales, B. Clevenger, R.S. Ruoff, Nano Lett. 12 (2012) 1806.
[37] W.T. Huang, H. Zhang, Y.Q. Huang, W.K. Wang, S.C. Wei, Carbon 49 (2011) 838.
[38] K. Fic, G. Lota, M. Meller, E. Frackowiak, Energy Environ. Sci. 5 (2012) 5842.
[39] L. Demarconnay, E. Raymundo-Piñero, F. Béguin, Electrochem. Commun. 12 (2010) 1275.
[40] M. Oschatz, L. Borchardt, K. Pinkert, S. Thieme, M.R. Lohe, C. Hoffmann, M. Benusch, F.M. Wisser, C. Ziegler, L. Giebeler, M.H. Rümmeli, J. Eckert, A. Eychmüller, S. Kaskel, Adv. Energy Mater. (2013) 1.